AIAA JOURNAL
Vol. 45, No. 7, July 2007

Tip Gap Effects on the Unsteady Behavior of a Tip Leakage Vortex

Ruolong Ma* and William J. Devenport†
Virginia Polytechnic Institute and State University, Blacksburg, Virginia 24061-0203

DOI: 10.2514/1.13536

The effects of tip gap on the unsteady behavior of a tip leakage vortex downstream of an idealized axial compressor rotor blade have been investigated in a linear cascade wind tunnel, extending the study of Ma and Devenport. The wind tunnel features a moving end wall to simulate the relative motion between the rotor and casing, and vortex generator pairs attached to the moving end wall that produce an idealized unsteady vortical inflow. Detailed three-component mean velocity and turbulence measurements have been made just downstream of the blade trailing edges for a series of tip gaps, from 0.83 to 3.3% chord, and phase averaged with respect to the relative position of the blades and vortex generator wakes, to reveal the structure of this flow and its dependence on tip gap. Significant fluctuations in the size, strength, structure, and position of the tip leakage vortex are produced by the vortical inflow even though it is one to two orders weaker than the tip leakage vortex. Interestingly, the amplitude of these effects increases with tip gap as the tip vortex strengthens. For small tip gaps, the disturbance to the leakage vortex appears to be a consequence of direct interaction with the inflow vortices. However, for larger tip gaps it is the indirect action of the inflow vortices interfering with the shedding of circulation from the blade tip that appears to be the dominant source of unsteadiness in the leakage vortex.

Introduction

THE rotor of an axial turbomachine often operates downstream of a set of fixed stators or inlet guide vanes. The wakes of the stators create an unsteady inflow that results in lift fluctuations on the rotor blades. Near the casing, where the incoming stator wakes are dominated by streamwise vorticity shed from the casing junctions, this interaction can produce unsteady motions of the rotor tip leakage vortices. Such motions are known to be associated with intermittent cavitation downstream of propulsion pump rotor blades. They are also likely to be associated with greater noise and vibration produced when the tip leakage vortices interact with downstream elements. One would expect the sensitivity of the leakage vortex to inflow disturbances to be strongly dependent on tip gap and, indeed, tip gap varies widely in various turbomachines (typically about 1% of the blade span for compressors or fans, and 3% for propulsion pumps). These effects of tip gap are the focus of this paper.

The literature contains few references to studies of the effects of stator–rotor interaction on tip leakage vortices [1–6]. Most of this work is focused only on the time average formation and development of the vortex and does not address the mechanism or consequences of the unsteady interaction. One exception are the flow visualizations of Zierke et al. [7,8] which show dramatic wandering and kinking of the cavitating tip leakage vortex as it passes downstream of the rotor-blade trailing edge, apparently in response to the stator–rotor interaction.

Previous studies of tip gap effects on tip leakage vortices in the absence of inflow disturbances have been conducted both on cascades and rotors. Storer and Cumpsty [9] studied tip gap effects on a compressor cascade and found that tip clearance vortex increases in size and strength as the clearance is increased. The vortex was not obvious for clearances less than 1% chord. For 2% chord its origin was traced to near the blade tip leading edge for 2% chord clearance and moved further downstream for larger clearance. Doukelis et al. [10] investigated the tip gap effects on the performance of a high-speed annular compressor cascade. The authors concluded that the size of the tip leakage vortex and associated losses in the hub clearance region increase with the tip gap size, and the location of minimum pressure on the blade tip suction side moves downstream with the increasing of the tip gap.

Two cascade studies, closely related to the present study, have provided more detailed information of tip leakage effects on the time-averaged form of the tip leakage vortex. Muthanna and Devenport [11] studied the structure of a tip leakage vortex and its trajectory downstream of the same General Electric (GE) rotor B compressor cascade used in the present study at tip gaps of 0.8, 1.6, and 3.3% chord. Muthanna and Devenport's measurements reveal that tip gap has a strong effect on the position, size, and rotational strength of the vortex. As tip gap is increased, the size and total circulation increase, and the vortex center moves across the end wall, away from the rest of the blade wake, due to the increase in mean rotational strength. However, the streamwise mean velocity deficit and the turbulence structure and intensity inside the vortex are unaffected by tip gap size. Tip gap effects were further studied by Wang and Devenport [12] on the tip leakage vortex in the same facility but with and without a moving end wall to simulate the relative motion of the blade tips and casing seen in a real turbomachine. They found that, although wall motion distorts the vortex and alters its mean trajectory, it does not substantially alter the mechanisms governing its turbulent decay or the effects of tip gap upon it.

Inoue et al. [13] studied the flow in an isolated axial compressor rotor and found, as the tip clearance rises, the tip leakage vortex is more intense. The position of its roll up also becomes more distant from the suction side of the blade and, however, changes little for tip clearances larger than 2% tip chord. A region of axially reversed flow is formed associated with the vortex grows. Inoue and Kuroumaru [14] measured ensemble-averaged and phase-locked flow patterns in the same rig. They found the leakage flow is stronger near the leading edge and interacts violently with the through flow for small clearances. For larger clearances a stronger leakage vortex is formed at a more downstream location and the vortex center path is more inclined toward the pitchwise direction. Goto [15] investigated flow in a single stage axial flow compressor and found that the size of the tip leakage vortex increases with the size of tip clearance while the

Received 20 September 2004; revision received 5 January 2007; accepted for publication 22 January 2007.

*Graduate Assistant, Department of Aerospace and Ocean Engineering, 215 Randolph Hall, Currently at Hessert Lab, University of Notre Dame. Senior Member AIAA.

†Professor, Department of Aerospace and Ocean Engineering, 215 Randolph Hall. Associate Fellow AIAA.

development of the hub viscous region and the broadening of the wake were suppressed due to the blockage effects. He also observed intense small-scale unsteadiness due to the diffusion of the tip leakage vortex at large tip clearances.

This paper follows on from the work presented by Ma and Devenport [16], Mish et al. [17] and Staubs et al. [18]. As in the present study, they used a linear cascade with adjustable tip gap to examine the study of stator/rotor interaction on tip leakage vortex structure. The cascade provides a large-scale leakage flow in a stationary frame of reference allowing detailed measurements of the phase-locked mean flow and turbulence structure. A moving end wall is used to correctly simulate the relative motion of the rotor blade tips and casing. Vortex generator pairs were attached to the moving end wall to produce an unsteady vortical inflow to the cascade. These inflow vortices simulate, in an idealized way, the streamwise vortical structures (such as the necklace and corner separation vortices) that would dominate the wakes of upstream stators near the stator/casing junctions.

Ma and Devenport [16], hereafter referred to as MD [16], presented phase-averaged measurements of the tip leakage flow downstream of a linear cascade at a single tip gap of 3.3% chord. The tip leakage vortex was periodically disturbed by the inflow vortices, shed by the vortex generators, with strength about two orders weaker than the tip leakage vortex. Although these had little effect on the time-averaged flowfield, phase-averaged measurements showed significant fluctuations in the size, strength, structure, and position of the tip leakage vortex. MD [16] hypothesized that the unsteady vortical inflow influences the tip leakage vortex at its formation, by periodically disturbing the shedding of vorticity from the blade tip.

Mish et al. [17] investigated the effects of tip gap on the unsteady blade tip surface pressure distribution. Measurements were made using an array of 24 embedded microphones in an extensive tip gap range from $0.83\%c$ to $12.9\%c$, where c is the total blade chord. Significant pressure fluctuations were found to be produced by the inflow disturbance and to increase in intensity with tip gap up to $5.7\%c$. Mish et al.'s results suggest a strong viscous component to the blade tip response traveling downstream at the trace speed of the inflow disturbances along the blade tip. Staubs et al. [18] further studied the correlation between the unsteady loading and tip gap flow and found that the disturbances to the unsteady tip gap mass flow and the pressure differences across the blade seem to follow the same general pattern. However, he observed a time lag between the pressure difference and mass flow, which increases with distance downstream.

The purpose of this paper is to present measurements of the unsteady tip leakage flow shed from an idealized compressor blade tip in the presence of periodic inflow disturbances. This work extends the results of MD [16] in showing the effects of tip gap on the phase-locked mean flow and turbulence structure, and provides insight into how the blade tip effects of Mish et al. [17] and Staubs et al. [18] influence the development of the vortex downstream. Detailed measurements reveal, for the first time, the exclusive effects of tip gap on the unsteady behavior of a tip leakage vortex, and further improve the understanding of the mechanisms that control the unsteady behavior of the vortex. More details of this study are described by Ma [19].

Apparatus and Instrumentation

Measurements were made in the same low-speed linear cascade facility described in detail by MD [16], and using the same three-component four-sensor hot-wire instrumentation and procedures. We therefore summarize here only the parameters of the facility and the measurement procedures and describe the information related to the tip gap adjustment. As shown in Fig. 1a, the heart of the wind tunnel is a cascade consisting of eight aluminum GE rotor B section blades. The blades were mounted with a stagger angle of 56.9 deg, an inlet angle of 65.1 deg, and a blade spacing s of 236 mm (a solidity of 1.08). The effective span of each blade is nearly the same as the chord length c of 254 mm, depending on the size of the tip gap. Natural transition is eliminated by 6.4-mm wide distributed roughness trips, attached to both sides of each blade 25.4 mm downstream of its leading edge. Tailboards were adjusted to a turning angle of 11.8 deg at which the flow was free from any net pitchwise pressure gradient. The nominal inlet freestream velocity U_∞ was 24.5 ± 0.5 m/s, corresponding to a chord Reynolds number at 27°C of $398,000 \pm 8100$.

Mounted on an aluminum superstructure, the eight cantilevered blades project through close-fitting shaped slots in the upper endwall and are held a short distance above the lower endwall, with this distance representing the tip gap (Fig. 1b). The lower endwall was covered by a 0.25 mm-thick Mylar belt running under the entire cascade and extending 125 mm axially upstream and 422 mm axially downstream of the blade row. The belt is propelled at a speed equal to the tangential component of the freestream so as to correctly simulate the relative motion between blade tip and casing experienced in an actual turbomachine. The flow approaching the tip gaps over the lower endwall was conditioned, as far as possible, to generate a tangentially uniform inlet boundary layer with inlet skew. A 2.5 mm high square trip wire was attached to the lower endwall 7 mm downstream of this suction slot to ensure the development of a turbulent boundary layer. This new boundary layer was allowed to grow over a stationary section of endwall 73.2 mm wide before flowing on to the moving Mylar surface. The boundary layer then continued to develop over the moving surface before encountering the blade row, the total width of the exposed moving belt here being 112.7 mm. The thickness of the endwall boundary layer entering the cascade, midway between the blade leading edges, was about 6 mm.

Half-delta wing vortex generator pairs were glued to the belt with their trailing edges 68.6 ± 4.5 mm upstream of the blade row. The vortex generator pairs were spaced 236 mm apart, a distance equal to the blade spacing. The 10-mm high generators were arranged to produce a common flow down the vortex pair. The leading vortex is larger with a height of $7\%c$ at $0.135s$ upstream of the cascade leading edge. The circulation is about $0.003U_\infty s$, which is 2 orders of magnitude smaller than the typical circulation in the tip leakage vortices in the cascade tunnel. Detailed measurements of these inflow disturbances are presented by MD [16].

An optical system was used to sense the instantaneous generator location and to construct a phasing signal by subdividing each time interval into 256 equal periods representing the instantaneous position of the vortex generator pairs relative to the blades. A photodetector was placed underneath the belt 81 mm axially upstream of the center point of the cascade leading-edge line of the central blade passage. At phase 0 generator pairs are positioned right over the photodetector, also exactly axially upstream of the center point of each blade passage entrance. At phase 128 generator pairs are located axially upstream of the blade leading edges. The position of the generator pairs at all 256 phases can thus be inferred. An increment in the phase number of 1 represents a tangential motion of the generators of $s/256$, that is, almost 1 mm.

The four-sensor hot-wire probe used to make phase-locked mean velocity and turbulence measurements consists of two orthogonal X-wire arrays with each sensor inclined at a nominal 45-deg angle to the probe axis. The total measurement volume is approximately 0.5 mm^3. Three velocity components were obtained by using a direct angle calibration method, described in detail by Wittmer et al. [20]. A computer-controlled two-axis traverse system with a resolution of 0.025 mm was used to position probes.

Results and Discussion

In presenting measurements we will use the cascade coordinates (X, y, Z) and downstream flow-aligned coordinates (x, y, z) illustrated in Fig. 1a. The origin of the cascade coordinates is on the lower endwall midway between the leading edges of the two center blades (nos. 4 and 5). The X axis is in the axial direction across the cascade, y lies perpendicular to the lower endwall, and Z is in the pitchwise direction. The downstream flow-aligned coordinates are

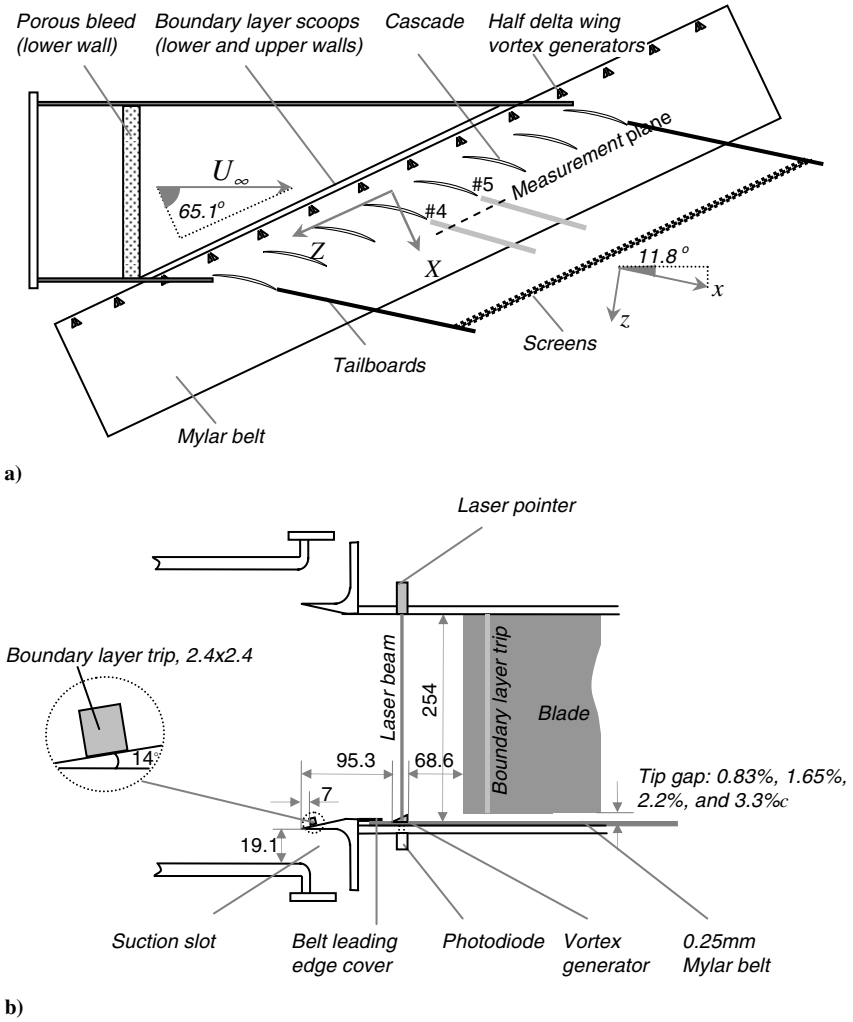

Fig. 1 a) Plan view of the Virginia Tech cascade wind tunnel test section; b) cross section through the cascade taken along the cascade axial direction. Dimensions in millimeters and not to scale.

rotated about the y axis compared to the cascade coordinates, the angle between X and x being 53.3 deg. Velocities are presented in terms of the components (u, v, w) aligned, respectively, with the downstream coordinates (x, y, z). Most velocities are normalized on the inlet freestream velocity U_∞. Most positions are normalized on the blade spacing s of 236 mm and chord c of 254 mm.

In the paper by MD [16], velocity and turbulence measurements downstream of the cascade at a single tip gap t/c of 3.3% were discussed. Here three additional sets of measurements are presented. These were made at similar locations to those examined by MD [16] but for tip gaps $t/c = 2.2$, 1.65, and 0.82%. Measurements were made both with and without inflow disturbances in cross-sectional planes at $X/s = 0.944$ for $t/c = 2.2$ and 0.82%, and at $X/s = 0.843$ (with disturbances) and $X/s = 0.896$ (without) for $t/c = 1.65\%$. The measurement planes were thus about 30%s axially downstream from the trailing edge plane at $X/s = 0.59$. Measurements were made on grids of points covering one passage width in the pitchwise direction and from the lower endwall to about $y/s = 0.6$ in the spanwise direction. As such the measurements encompass the complete endwall region including the tip leakage vortex as well as a substantial portion of the potential core and two-dimensional region of the blade wakes. Close to the endwall a detailed grid of points was used to resolve the unsteady vortex structure here. With inflow disturbances, measurements in this near wall region were made by taking 100 records of 16,384 samples of each of the four hot-wire signals and the generator position signal at a rate of 25.6 kHz. The total number of samples was chosen so that the phase averages could be estimated from data representing at least 5000 vortex generator pair passes. Elsewhere, and without inflow disturbances, only time-averaged statistics were required. In these cases measurements were made by taking a single record of 10,240 samples of the signals at a rate of 1600 Hz.

Time average velocity and turbulence measurements will be presented first to show the overall flow structure and its dependence on the tip gap. Phase-averaged results will then be presented, followed by integrated quantities designed to show the fluctuations in the strength of the tip leakage vortex induced by the unsteady vortical inflow. Uncertainties in time average and phase average measurements were calculated for 20:1 odds using the method of Kline and McClintock [21] and the results are listed in Table 1.

Time-Averaged Results

Without Inflow Disturbances

Time-averaged measurements made without inflow disturbances are presented in Figs. 2–4 in terms of contours of mean streamwise velocity, turbulence kinetic energy (TKE), and streamwise vorticity. Streamwise vorticity was calculated by numerical differentiation of the mean velocity data ignoring derivatives on the flow (x) direction. In each figure, three tip gaps, $t/c = 2.2$, 1.65, and 0.83%, are shown. Results for the fourth tip gap (3.3%) are shown in comparable form by MD [16]. Problems with the measurements made without inflow disturbances for $t/c = 1.65\%$ rendered them unusable so, in their place, we present here the data of Wang and Devenport [12] measured at the same location for almost the same flow. The only difference in conditions for Wang and Devenport's measurements was a shorter length of endwall upstream of the cascade and thus a slightly thinner inlet boundary layer. Figures 2–4 show the flow as it

Table 1 Measurement uncertainties for both time- and phase-averaged measurements

Quantity	Uncertainties (20:1 odds)
$\delta U/U_\infty$	1%
$\delta(V, W)/U_\infty$	0.7%
$\delta(\overline{u'^2}, \overline{v'^2}, \overline{w'^2})/U_\infty^2$	0.01%, 0.08%, 0.1%
$\delta(\overline{u'v'}, \overline{v'w'}, \overline{u'w'})/U_\infty^2$	0.005%, 0.03%, 0.02%
$\delta k/k$	6%
$\delta(\Omega_x)/\Omega_x$	18%

would appear from upstream so that the direction of the endwall motion is from right to left.

These figures show overall flow patterns similar to that seen at the larger $3.3\%c$ tip gap by MD [16]. The vertical wakes shed from blades 5 and 4 are visible, respectively, on the left- and right-hand edges of each figure. The tip leakage vortex, shed from blade 4 and the associated boundary layer flow, is contained within the flattened oval region at the bottom of these figures. It is seen intersecting with the wake of blade 5, having convected across the passage. The contours of mean velocity (Fig. 2) show the vortex to be associated with a region of strong streamwise mean velocity deficit. The peak deficit is about twice the deficit in the two-dimensional portions of the blade wakes. As discussed by MD [16] the location of the peak deficit provides a useful definition of the center of the vortex. This vortex is dominated by its streamwise velocity deficit because of the light loading of the cascade blades.

As the tip gap is increased the deficit region associated with the vortex changes location (shifting closer to blade 5 as it drifts further across the endwall) and increases in size. The height of this region increases from about $0.18s$ at $t/c = 0.83\%$ to $0.22s$ at $t/c = 2.2\%$,

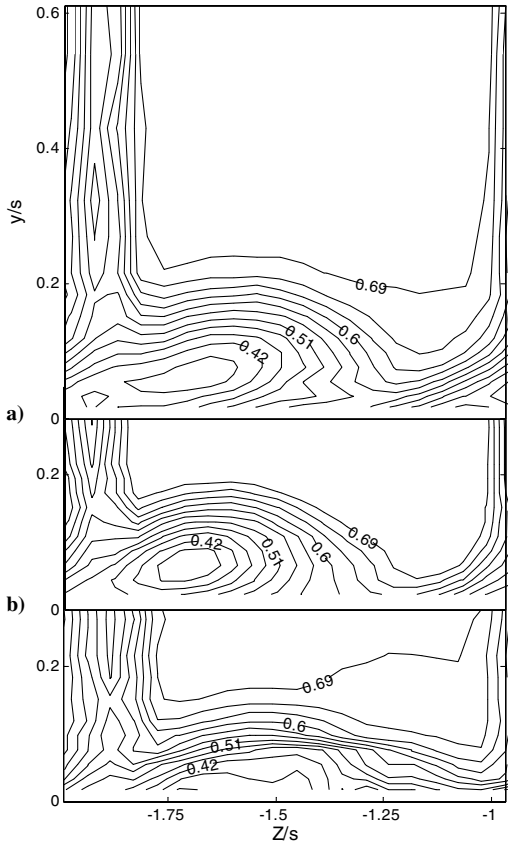

Fig. 2 Contours of time-averaged streamwise velocity U/U_∞ without vortex generators. Contours in steps of 0.03. a) $t/c = 2.2\%, X/s = 0.944$; b) $t/c = 1.65\%$, $X/s = 0.896$ (Wang and Devenport [12]); c) $t/c = 0.83\%, X/s = 0.944$.

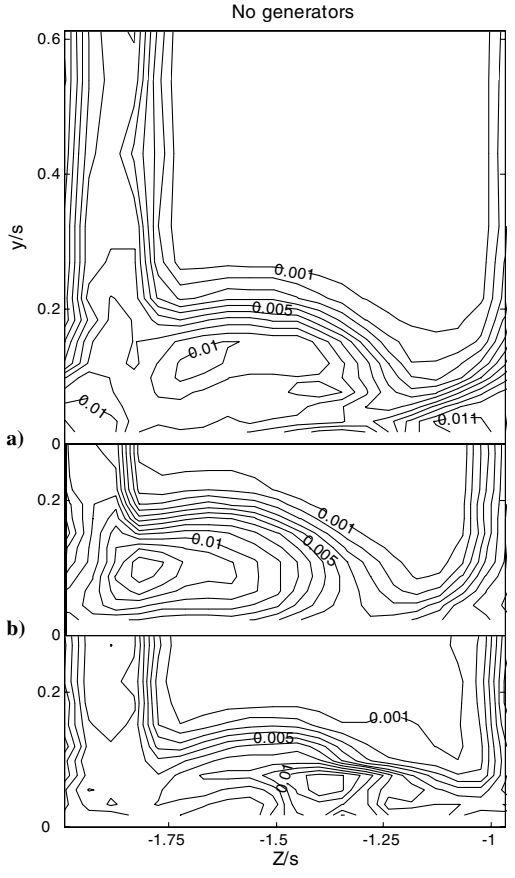

Fig. 3 Contours of time-averaged turbulence kinetic energy k/U_∞^2 without vortex generators. Contours in steps of 0.001. a) $t/c = 2.2\%$, $X/s = 0.944$; b) $t/c = 1.65\%$, $X/s = 0.896$ (Wang and Devenport [12]); c) $t/c = 0.83\%$, $X/s = 0.944$.

and then to $0.25s$ for $t/c = 3.3\%$ (as shown in Fig. 7a of [16]). Despite these substantial changes the maximum streamwise velocity deficit in the vortex remains almost constant varying only from $0.36U_\infty$ for $t/c = 0.83\%$ to $0.34U_\infty$ for $t/c = 3.3\%c$. This same invariance with tip gap was seen previously further downstream of the cascade by Muthanna and Devenport [11] (without endwall motion) and Wang and Devenport [12] (with endwall motion).

Figure 3 shows turbulence kinetic energy patterns in the vortex region are quite different at the different tip gaps. For $t/c = 0.83\%$ the TKE peaks near $Z/s = -1.6$ adjacent to the endwall near the region of maximum streamwise velocity deficit, and also to the right of and above that region, around $Z/s = -1.4$. For $t/c = 1.65\%$ only a single maximum is visible, centered close to the location of the peak streamwise velocity deficit. With $t/c = 2.2\%c$ TKE reaches its largest values just above the center of the deficit generated by the vortex (near $Z/s = -1.7$), and also close to the endwall underneath the intersection of the wake and vortex regions around $Z/s = -1.9$. A structure similar to $t/c = 2.2\%c$ is seen for $t/c = 3.3\%$ in Fig. 9a of [16]. The multiple peaks seen at these larger tip gaps are believed to be due to the interaction of the vortex and the wake of blade 5. Despite these fairly dramatic changes in structure the peak TKE levels themselves remain surprisingly constant around $0.012U_\infty^2$ for all tip gaps (again consistent with observations of Muthanna and Devenport [11] and Wang and Devenport [12]). The slightly higher peak TKE of $0.013U_\infty^2$ for $t/c = 1.65\%$ is perhaps because the measurement location $X/s = 0.896$ in this case was $0.048s$ further upstream than for the other tip gaps. A rate of decay consistent with this difference was seen for $t/c = 3.3\%c$ in the results of [16].

The contours of mean streamwise vorticity in Fig. 4 for $t/c = 0.83$, 1.65, and 2.2% show some similarity with those of mean velocity and TKE, particularly in the pitchwise location and

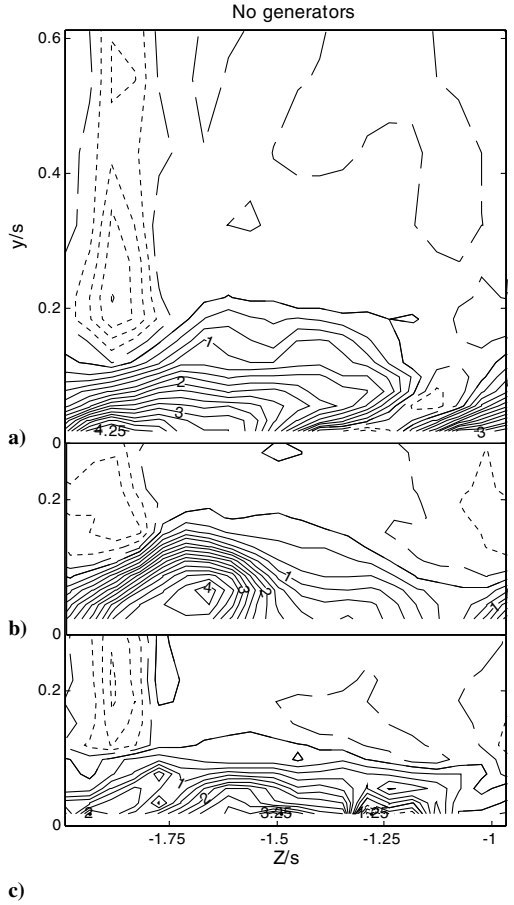

Fig. 4 Contours of time-averaged streamwise vorticity $\Omega_x s/U_\infty$ without vortex generators. Dotted, dashed, and solid lines show negative, zero, and positive levels, respectively. Contours in steps of 0.25. a) $t/c = 2.2\%$, $X/s = 0.944$; b) $t/c = 1.65\%$, $X/s = 0.896$ (Wang and Devenport [12]); c) $t/c = 0.83\%$, $X/s = 0.944$.

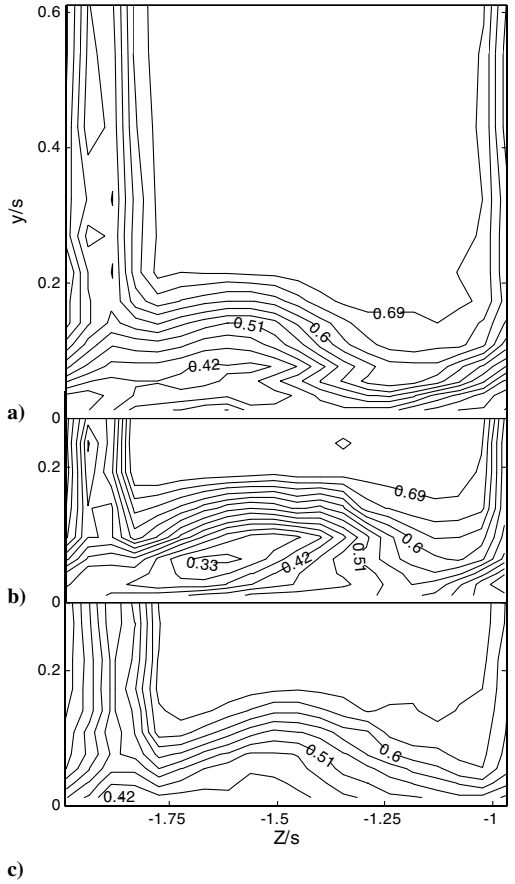

Fig. 5 Contours of time-averaged streamwise velocity U/U_∞ with vortex generators. Contours in steps of 0.03. a) $t/c = 2.2\%$, $X/s = 0.944$; b) $t/c = 1.65\%$, $X/s = 0.843$; c) $t/c = 0.83\%$, $X/s = 0.944$.

organization of most of the most prominent features associated with the blade wakes and leakage vortex. At all tip gaps, however, the most intense streamwise vorticity is not found near the vortex center (as observed in the streamwise mean velocity deficit) but closer to, if not at, the endwall. The reason for this is that shearing between the flow out of the cascade and the pitchwise moving endwall is itself associated with intense streamwise vorticity of the same sign as the leakage vortex. This additional streamwise vorticity obscures the leakage vortex and shifts regions of highest vorticity toward the endwall. Under these combined effects the peak streamwise vorticity increases with tip gap from $3.4U_\infty/s$ for $t/c = 0.83\%$ to $4.5U_\infty/s$ for $t/c = 2.2\%$ while the peak streamwise vorticity for $t/c = 3.3\%$ is, however, $3.8U_\infty/s$, which is different from those shown in mean velocity and TKE. Overall, Figs. 2–4 show a flow structure closely consistent with the findings of Muthanna and Devenport [11] and Wang and Devenport [12].

Effects of Inflow Disturbances

Time-averaged measurements made with the periodic vortical inflow disturbance present are shown in Figs. 5–9. The inflow disturbances have a fairly subtle effect on the mean streamwise velocity distributions (Fig. 5). In the endwall region occupied by the vortex these become slightly more elongated in the pitchwise direction, perhaps indicating coherent pitchwise motions of the vortex. Also, the inflow vortices seem to result in some filling in of the potential core region found near the endwall, between the vortex and wake of blade 4 (around $Z/s = -1.15$). There is a slight reduction in the streamwise velocity deficit due to the presence of the unsteady inflow compared with Fig. 2, except for the $1.65\%c$ tip gap case for which the two sets of data were taken at slightly different locations. Mean crossflow velocity vectors shown in Fig. 6 display a similar vortical flow pattern at all tip gaps, but the leakage flow obviously grows in size and magnitude of the crossflow velocity components as the tip gap is increased.

The contours of TKE in Fig. 7a show a slight increase of both level and extent in the vortex core region with inflow disturbances for the tip gap of $2.2\%c$. The core structure, especially the location of the peak TKE within the vortex core, is also altered, the peak moving from near $Z/s = -1.7$ to -1.5 and closer to the endwall. TKE levels adjacent to the endwall remain large, however, and comparable to the highest levels in the vortex. This is unlike the $3.3\%c$ tip gap case for which inflow disturbances were found to enhance peak TKE levels in the vortex core compared to those near the endwall (see Fig. 9b of MD [16]). For the smaller tip gaps (Figs. 7b and 7c), the inflow disturbances actually decrease in magnitude of peak TKE, compared with Fig. 3c. As with that of the mean streamwise velocity, the distribution of TKE is visibly elongated in the pitchwise direction by the inflow disturbances, particularly for the smaller tip gaps. A similar "filling in" of the potential core between the vortex region and wake of blade 4 is also seen. These effects could be an indication of pitchwise meandering of the vortex induced by the inflow disturbances, which would tend to stretch its appearance in that direction.

The effects of the inflow disturbances on the mean streamwise vorticity can be seen by comparing Figs. 4 and 8. The strong vorticity levels in the vicinity of the endwall associated with the no-slip condition and moving endwall are little influenced by the inflow disturbances. Away from the wall the same elongation of the flow structure seen in the other measurements is visible. This change in structure is most clearly seen for the $1.65\%c$ tip gap, where the single concentrated region of vorticity seen around $Z/s = -1.7$ without inflow disturbances appears distributed across most of the endwall, when the disturbances are added.

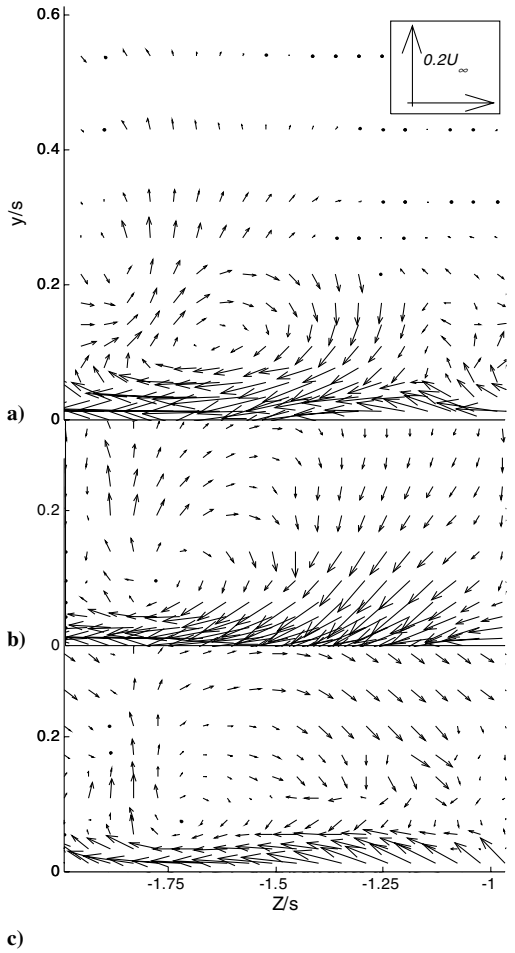

Fig. 6 Contours of time-averaged crossflow velocity (V, W). a) $t/c = 2.2\%$, $X/s = 0.944$; b) $t/c = 1.65\%$, $X/s = 0.843$; c) $t/c = 0.83\%$, $X/s = 0.944$.

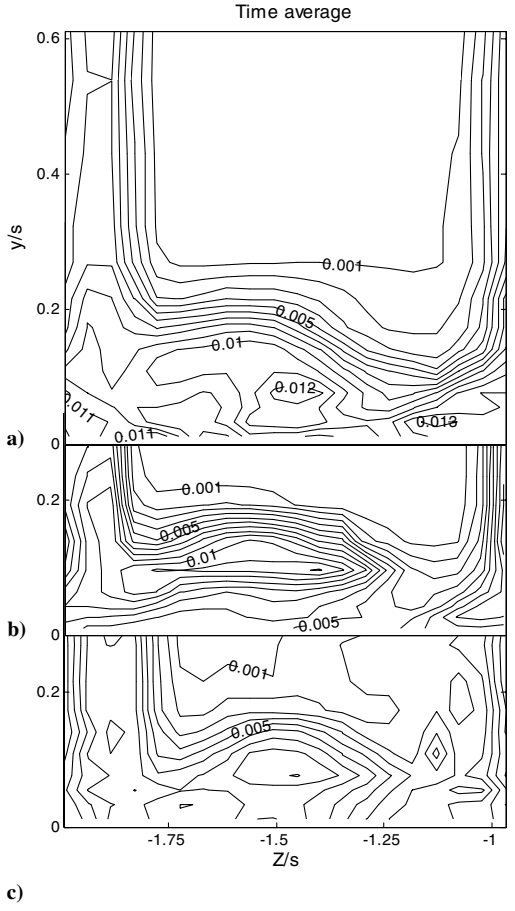

Fig. 7 Contours of time-averaged turbulence kinetic energy k/U_∞^2 with vortex generators. Contours in steps of 0.001. a) $t/c = 2.2\%$, $X/s = 0.944$; b) $t/c = 1.65\%$, $X/s = 0.843$; c) $t/c = 0.83\%$, $X/s = 0.944$.

Figure 9 summarizes the effects of tip gap and inflow disturbances upon the parameters of the time average leakage vortex flow. Shown here are the overall height of the vortex (measured to the height of the $0.001U_\infty^2$ turbulence kinetic energy contour) and the peak mean streamwise velocity deficit, turbulence kinetic energy, and streamwise vorticity measured in the endwall region. In terms of these parameters, the effects of tip gap on the leakage vortex in the presence of inflow disturbances appear similar to those seen without inflow disturbances. The size of the tip leakage vortex still increases with the tip gap, and the maximum streamwise velocity deficit still appears unaffected by the tip gap except that it is reduced for the smallest tip gap of $0.83\%c$. (The higher value of the tip gap $1.65\%c$ case is because of a further upstream measurement location.) However, there are differences too. Peak TKE levels, which are almost constant with tip gap without inflow disturbances, show about a 50% increase with tip gap when inflow disturbances are present (consistent with observations to be made below). Streamwise vorticity levels appear lower with inflow disturbances at all tip gaps, except $2.2\%c$.

Phase-Averaged Results

Phase-averaged results presented in Figs. 10–13 show the cross-sectional structure of the flow at eight equally spaced phases (0, 32, 64, 96, 128, 160, 192, and 224) during one period of the interaction between the inflow disturbances and the cascade. The pitchwise position of the closest pair of vortex generators producing the inflow disturbances is shown on each plot as a pair of right triangles on the horizontal axis representing the axial projection of the generator pair. Complete sets of phase-averaged results including all 256 phases are available from Ma [19] as movies.

Because of the large number of plots involved, phase-averaged cross-sectional results are only presented here for tip gaps of $1.65\%c$ and $0.083\%c$. These can be compared with similarly plotted results for $3.3\%c$ presented by MD [16].

Contours of phase-averaged streamwise velocity and TKE for a tip gap $1.65\%c$ are presented in Figs. 10 and 11. From these plots it is quite obvious that significant phase average effects are present at this tip gap too. The streamwise velocity contours (shown in Fig. 10) reveal changes in the structure of the vortex with phase, particularly close to the endwall, though these effects are not as large as those of the $3.3\%c$ tip gap case [16]. It is surprising that reducing the tip gap reduces the unsteady effects, even though this goes a long way in explaining why the peak time average TKE levels in the vortex decrease with tip gap in the presence of inflow disturbances. A smaller tip gap produces a weaker tip leakage vortex and thus the relative strength of the inflow vortices is greater. This is a clear indication that the inflow disturbances do not influence the vortex in a linear way.

The flow around the center of the vortex streamwise velocity deficit (close to $Z/s = -1.4$) remains fairly stable except for a small decrease in the deficit around phase 192 shortly after the vortex generators pass in front of the locations. Slightly larger effects are seen in the flow to the right of the vortex (around $Z/s = -1.1$) in the region of the pitchwise velocity-gradient adjacent to the endwall. The magnitude of this gradient and its position both fluctuate as the disturbance passes (compare 128 and 224, for example). During the early phases (0 and 32) the TKE contours (Fig. 11) show two peaks, located on either side of the vortex, joined by an arch-shaped ridge. As the vortex generators move across the endwall, the left-hand TKE peak decays, and the right-hand peak intensifies (phases 64 and 96). At the same time, the left-hand peak moves in the negative Z direction to about $-1.6s$ at phase 96. Turbulence levels then decay

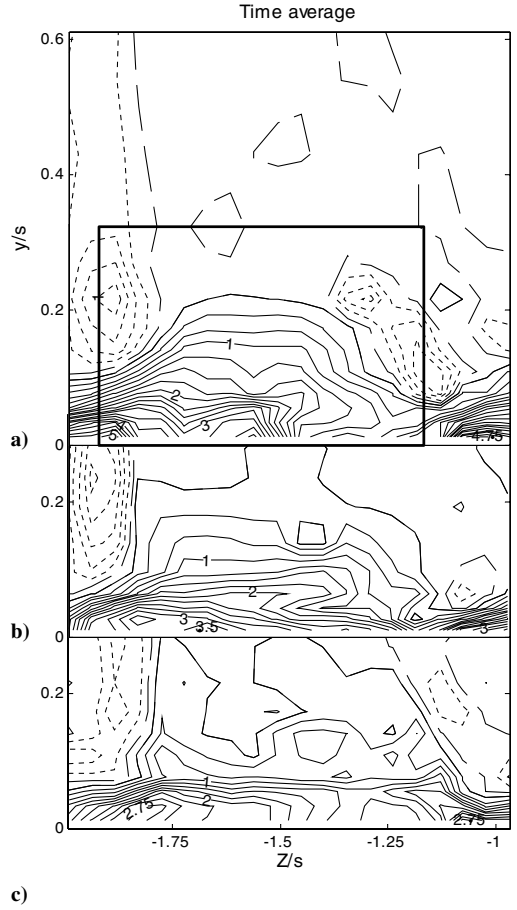

Fig. 8 Contours of time-averaged streamwise vorticity $\Omega_x s/U_\infty$ with vortex generators. Dotted, dashed, and solid lines show negative, zero, and positive levels, respectively. Contours in steps of 0.25. a) $t/c = 2.2\%$, $X/s = 0.944$; b) $t/c = 1.65\%$, $X/s = 0.843$; c) $t/c = 0.83\%$, $X/s = 0.944$.

(phases 96, 128, 160, and 192) and turbulence becomes redistributed over the arch-shaped ridge, ultimately reforming the original two peaks (phases 224 and 0). Phase-averaged mean crossflow velocity vectors [16] show that these effects are accompanied by a number of change structures, particularly in the region between $Z/s = -1.6$ and -1.75.

Figures 12 and 13 show the contour plots of streamwise velocity and TKE for the $0.83\%c$ tip gap case. Some of the phase average effects seen at this tip gap show a tendency to move across the endwall at almost the same speed as the vortex generators. An example in the phase-averaged streamwise velocity contours is the velocity minimum located at $Z/s = -1.55$ at phase 0 when the generator pair is centered at $Z/s = -1$. This minimum moves across the endwall to near $Z/s = -1.88$ at phase 128 by which time the generator pair has moved to $Z/s = -1.5$. The minimum then decays away. A similar feature seen in the phase-averaged TKE contours of Fig. 13 is the peak located at $Z/s = -1.4$ and $y/s = 0.12$ at phase 0 when the generator pair is at $Z/s = -1$. This peak moves $Z/s = -1.88$ and $y/s = 0.47$, underneath the wake of blade 5, at phase 160 at which time the generator pair is at $Z/s = -1.63$. In the meantime, a new peak is already in the process of being formed at around $Z/s = -1.4$.

The nature of these moving features is clearest in the phase-averaged vorticity field. Figure 14 shows three-dimensional isosurfaces of the vortex aligned streamwise vorticity at a level of $1.5U_\infty/s$ for the 0.83, 1.65, and 2.2% chord tip gaps. The isosurfaces are plotted as a function of pitchwise, spanwise distance and a representing streamwise distance ($-\Delta t U_e/s$) inferred from phase time Δt with Taylor's hypothesis assumed, where U_e is the potential core velocity. A total time span corresponding to two generator passage periods is plotted. Expected inflow vortex trajectories (assuming they convect axially downstream from the generators) are indicated by the arrows.

The comparable plot for the $3.3\%c$ tip gap, presented in Fig. 14 of [16], shows the main leakage vortex centered on $Z/s = -1.75$ undergoing a strong sinuous motion under the action of the inflow disturbances. The inflow vortices have no visible impact on the vorticity distribution. MD [16] argue that this motion is produced indirectly, by the action inflow disturbances on the shedding of vorticity from the cascade blade tips. Results shown in the present Fig. 14 suggest a change in behavior as the tip gap is reduced. At $t/c = 2.2\%c$ (Fig. 14a) the vortex and its sinuous motions are still visible but small vortical structures aligned with the expected inflow vortex trajectories are also seen near $Z/s = -1.7$. At $t/c = 1.65\%c$ and $0.83\%c$ (Figs. 14b and 14c) the sinuous motions are even less pronounced (if visible at all) and the vorticity isosurfaces show clear projections and indentations aligned with the expected inflow vortex trajectories. The implication is that, at small tip gaps, the direct influence of the inflow disturbances upon the tip leakage vortex may dominate over the indirect effects suggested by MD [16].

MD [16] found that the location of the maximum phase-averaged streamwise mean velocity deficit could be used quite successfully to track the center of the leakage vortex under the influence of the inflow vortices for a tip gap of $3.3\%c$. Using the same method we present here, the vortex center location as a function of the phase number is determined from the phase-averaged streamwise velocity data for $t/c = 0.83$, 1.65, and 2.2%. Results for all tip gaps are compared in Fig. 15. For the $3.3\%c$ tip gap, the vortex center follows a diagonal path, with the vortex center appearing near $\Delta Z/s = 0.09$ at phase 220, moving down and disappearing near $\Delta Z/s = -0.18$ at phase 219. With this motion being repeated the vortex center would be seen to follow a zigzag path. For the $2.2\%c$ and 1.65% tip gap cases, the vortex center location also moves in the pitchwise direction but less dramatically (over a range of about $0.15s$) and does not appear and disappear. For the smallest tip gap of $0.83\%c$, larger variations of the vortex center location are seen again, although there are two diagonal excursions and two disappearances and appearances of the vortex center) in each phase cycle. An explanation of this phenomenon might be that at large tip gap the shedding of the vorticity from the blade tip is periodically influenced by the vortical inflow. At lower tip gaps, this influence is weakened. When the tip gap gets very small ($0.83\%c$), not only the shedding of the tip leakage vortex is affected by the vortical inflow but also the tip leakage vortex itself is greatly influenced by the vortical inflow.

Tip Leakage Vortex Circulation Fluctuations

The phase-averaged circulation of the tip leakage vortex was calculated by clockwise integration of the velocity field along a rectangular path (shown in Fig. 8a), which was chosen to enclose the main tip leakage vortex. For the $3.3\%c$, $2.2\%c$, and $0.82\%c$ tip gap cases, the rectangular path extends from $(y/s, Z/s) = (0, -1.88)$ to $(0.32, -1.13)$, whereas for the $1.65\%c$ tip gap case, the rectangular path extends from $(y/s, Z/s) = (0, -1.72)$ to $(0.32, -0.97)$. The box was shifted in this case because of the difference in the streamwise location of the measurement plane. The calculated mean circulation of the tip leakage vortex for the $3.3\%c$ tip gap is $0.23U_\infty s$ which is about 80 times larger than the strength of the inflow vortices, $0.003U_\infty s$.

Results for the phase-averaged less time-averaged circulation are shown in Fig. 16. The circulation of the inflow vortices is also indicated in the figure for comparison. The inflow vortices have a nonlinear effect on the circulation of the tip leakage vortex. For the $0.82\%c$ tip gap case, the amplitude of fluctuations in the tip leakage vortex circulation with phase number is almost equal to the inflow vortex strength. This would be consistent with the fluctuations being produced by direct interaction, that is, superposition, between the inflow vortices and the tip leakage vortex. However, as the tip gap increases, the amplitude of circulation fluctuations in the

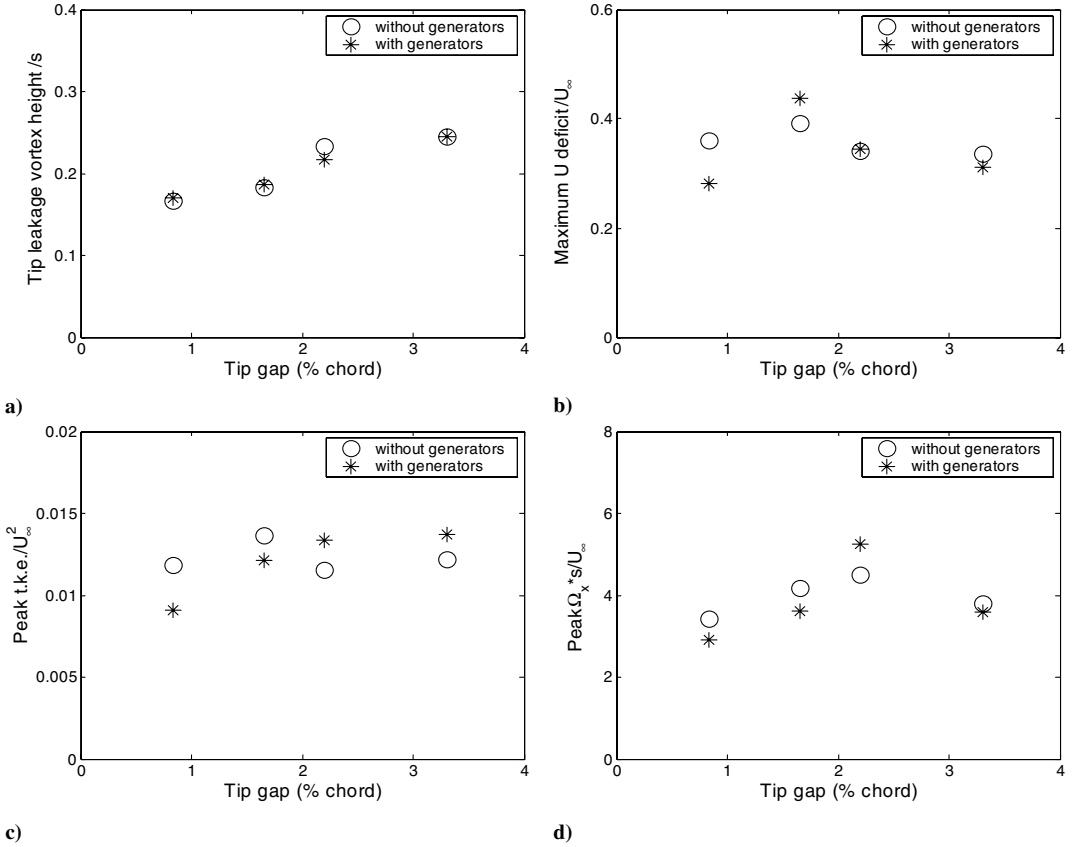

Fig. 9 Tip gap effects on some time average parameters of the tip leakage vortex with and without generators. a) Vortex height; b) maximum streamwise velocity deficit; c) peak turbulence kinetic energy; and d) peak streamwise vorticity.

leakage vortex increases in magnitude to values well above the strength of the inflow vortices. The maximum amplitude of fluctuation, for the 3.3%c tip gap case, is nearly 7 times the strength of inflow vortices. Obviously, such large fluctuations cannot be explained by superposition. The only source for additional vorticity needed to account for these large circulation fluctuations is the blade tip. Specifically, as hypothesized by MD [16] the inflow vortices must be modulating the shedding of vorticity from the blade tips.

Based on the blade surface pressure data of Ma [19], we would expect the total mean circulation at the middle span of the blade to be close to $0.25U_\infty s$. So supposing the phase-averaged fluctuation in the circulation of the tip leakage vortex comes from the unsteady circulation shedding at the blade tip, there must be significant variation (7.2% of the mean loading for 3.3%c tip gap) on the lift produced by the blades at the blade tip. Mish et al. [17] calculated the unsteady loading or circulation on the blade tip section ($y/s = 0.042$) due to the periodic inflow upwash presented by MD [16] by using Glegg's inviscid theory [22]. The theory assumes the blades are a flat plane with finite chord but extend in the spanwise direction to infinity. The tip gap effect is accounted by taking the upwash to be zero over the tip gap region. It was found that the unsteady circulation fluctuation on the blade tip section is on the same order of magnitude as the measured downstream tip leakage vortex circulation fluctuation. This suggests that the inviscid theory may produce useful results for predicting the broadband noise. Mish et al. also conducted unsteady blade loading measurements at the same facility to study the cascade blade response under the periodic inflow disturbance by using an array of 24 microphones mounted subsurface. The magnitude of measured fluctuations in the blade pressure response is found to increase with tip gap up to 5.7%c, which is consistent with the current study. However, the measured unsteady blade loading did not agree with the inviscid prediction very well. It seems the interaction appears to be heavily influenced by viscous forces. The viscous forces and inviscid response appear to work together to produce the large fluctuations in the tip leakage vortex circulation.

Conclusions

Extensive phase- and time-averaged turbulence measurements have been made to reveal tip gap effects on the unsteady behavior of a tip leakage vortex downstream of a simulated stator–rotor interaction. This interaction was produced in a linear cascade wind tunnel that features a moving endwall system with attached vortex generators to produce periodic inflow disturbances. Measurements of the leakage vortex were made some 30% of the blade spacing downstream of the trailing edge plane for tip gap sizes from 0.83%c to 3.3%c.

Without inflow disturbances the effects of tip gap on the leakage vortex are closely consistent with Muthanna and Devenport [11] and Wang and Devenport [12]. Increasing tip gap increases the size of the vortex and shifts the vortex in the pitchwise direction. There are also substantial changes in the turbulence structure of the vortex, in part because the pitchwise movement of the vortex brings it into contact with the wake shed by an adjacent blade. Despite these changes the peak turbulence kinetic energy and the peak streamwise mean velocity deficit in the vortex are almost unaffected by the tip gap.

The presence of inflow disturbances has a small noticeable impact on the vortex structure which becomes slightly elongated in the pitchwise direction, perhaps indicating coherent pitchwise motions of the vortex. Peak TKE levels in the vortex behave differently with inflow disturbances, increasing by about 50% from a tip gap of 0.83%c to 3.3%c. Consistent with this effect, phase-averaged measurements show unsteady motions of the leakage vortex which, at least at larger tip gaps (1.65%c and greater), increase in magnitude with tip gap.

At larger tip gaps (2.2% and 3.3%c) these motions include changes in position and structure of the leakage vortex and the

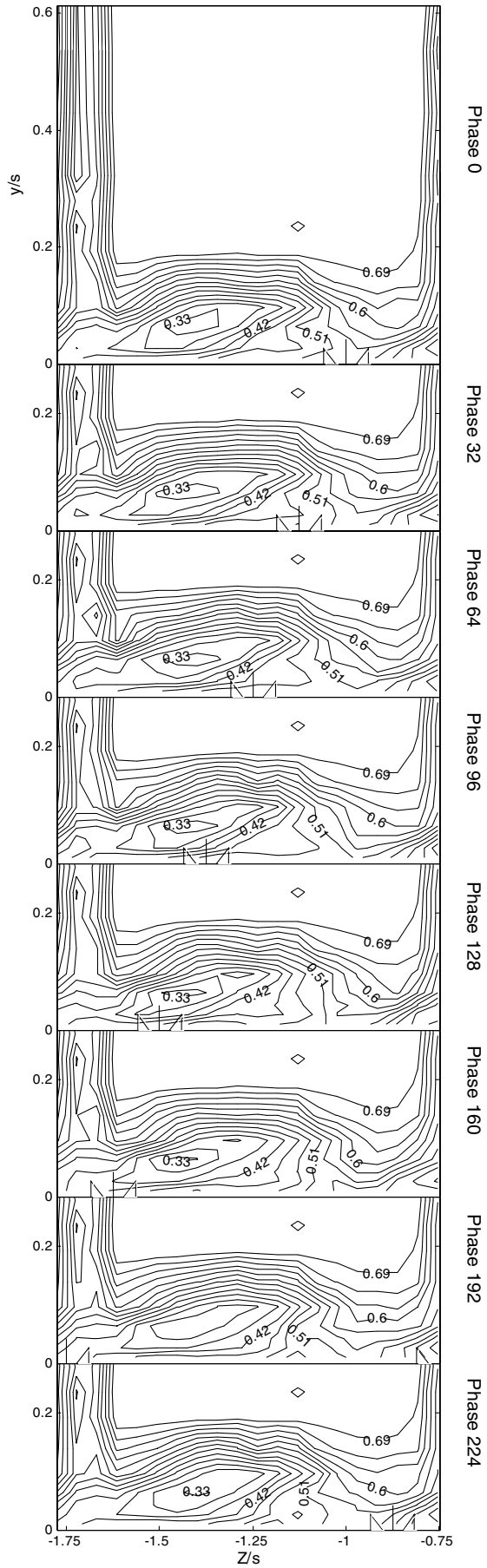

Fig. 10 Contours of phase-averaged streamwise velocity U/U_∞ with vortex generators for $t/c = 1.65\%$, $X/s = 0.843$. Contours in steps of 0.03. The triangle pairs indicate the pitchwise location of the vortex generators given in the table.

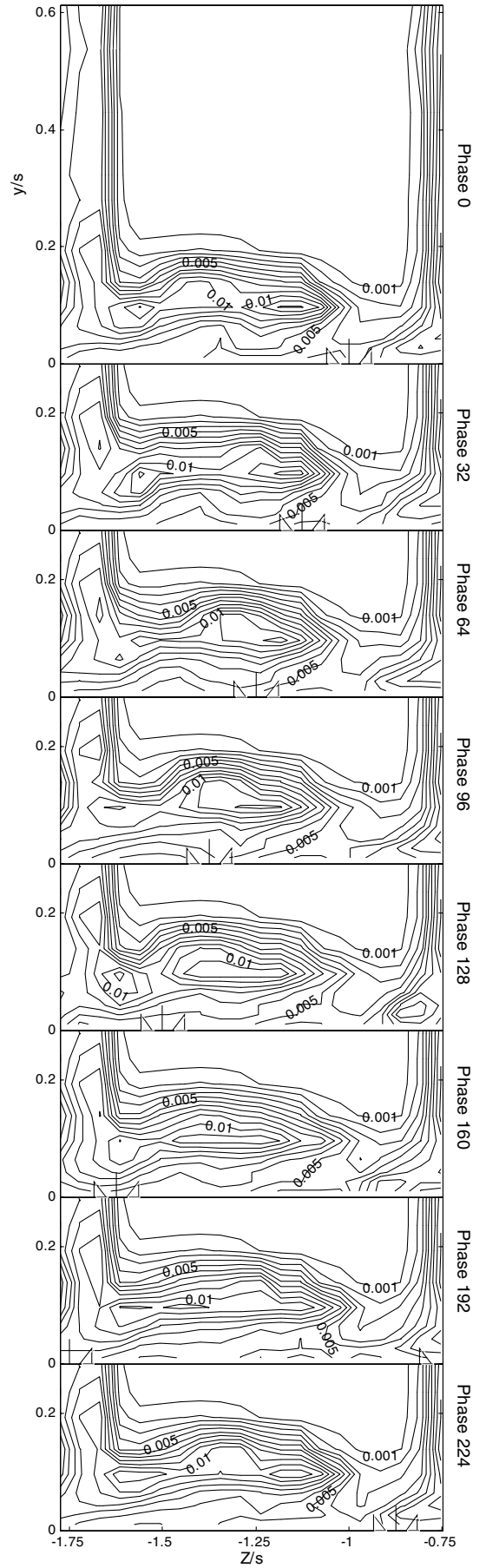

Fig. 11 Contours of phase-averaged turbulence kinetic energy $\langle k \rangle / U_\infty^2$ with vortex generators for $t/c = 1.65\%$, $X/s = 0.843$. Contours in steps of 0.001. The triangle pairs indicate the pitchwise location of the vortex generators as in Fig. 10.

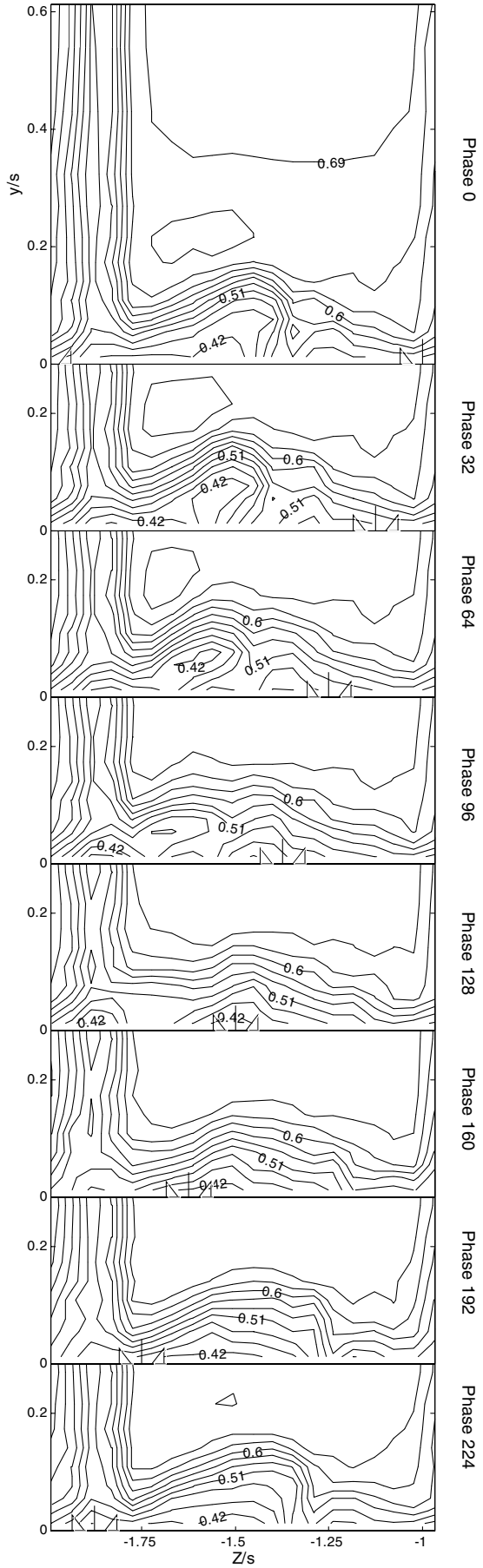

Fig. 12 Contours of phase-averaged streamwise velocity U/U_∞ with vortex generators for $t/c = 0.83\%$, $X/s = 0.944$. Contours in steps of 0.03. The triangle pairs indicate the pitchwise location of the vortex generators as in Fig. 10.

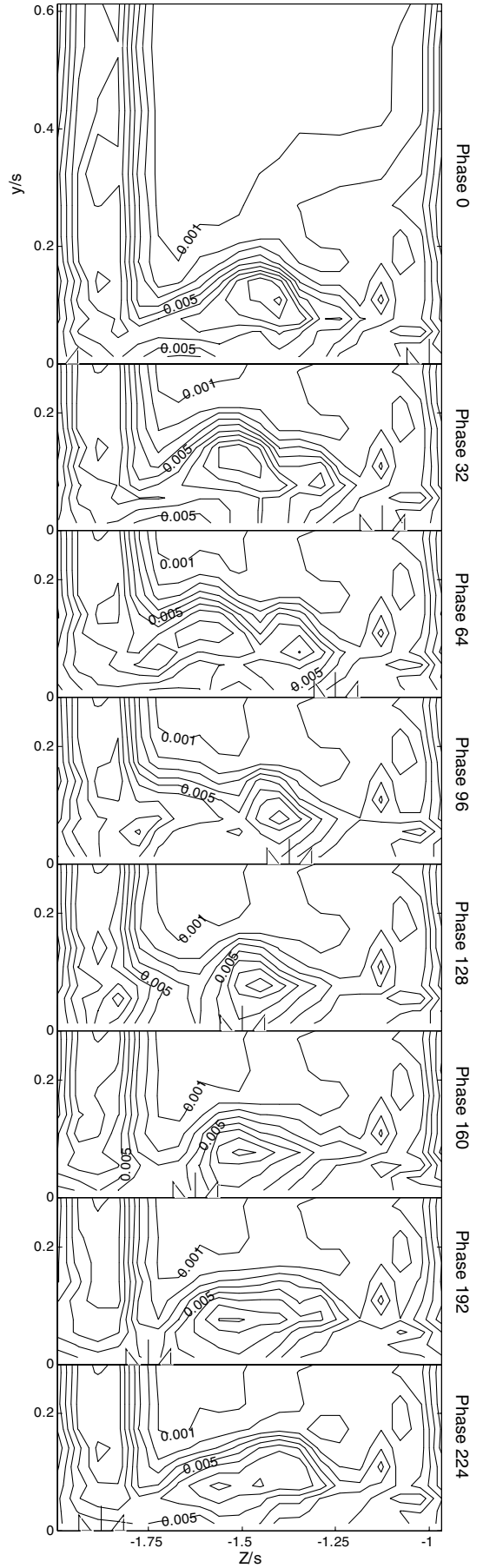

Fig. 13 Contours of phase-averaged turbulence kinetic energy $\langle k \rangle / U_\infty^2$ with vortex generators for $t/c = 0.83\%$, $X/s = 0.944$. Contours in steps of 0.001. The triangle pairs indicate the pitchwise location of the vortex generators as in Fig. 10.

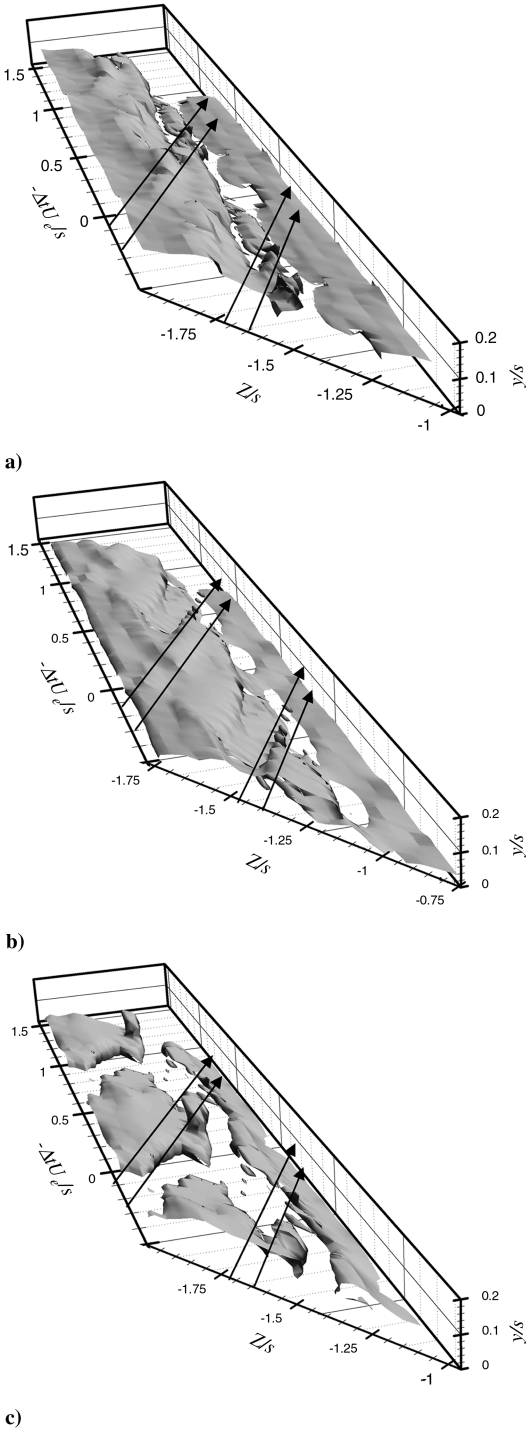

Fig. 14 Isosurfaces of phase-averaged vortex aligned streamwise vorticity of a level of $1.5U_\infty/s$. a) $t/c = 2.2\%$, $X/s = 0.944$; b) $t/c = 1.65\%$, $X/s = 0.843$; c) $t/c = 0.83\%$, $X/s = 0.944$.

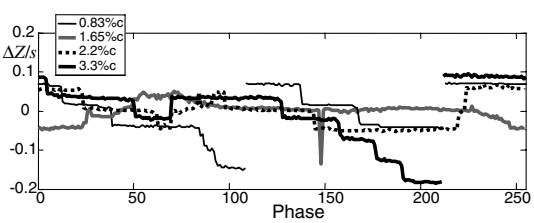

Fig. 15 Fluctuations in the pitchwise position of the primary tip leakage vortex center $\Delta Z/s$, indicated by maximum streamwise velocity deficit for all four tip gaps.

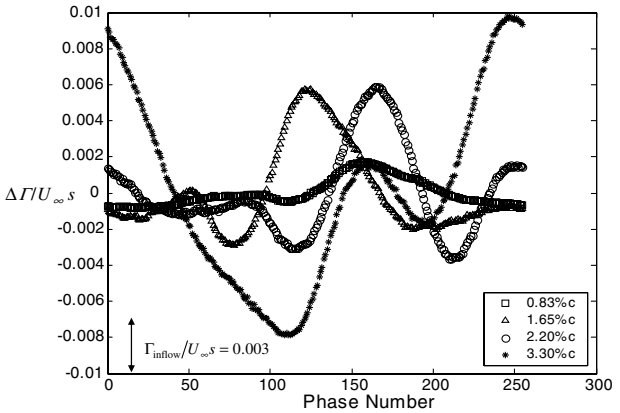

Fig. 16 Fluctuations in the circulation of the tip leakage vortex for four different tip gaps, calculated by integrating velocity along the rectangular path shown in Fig. 8a, and compared with the circulation of the strongest side of the inflow vortex pair.

turbulence generation within it and fluctuations in the vortex circulation with amplitudes many times the circulation of the inflow disturbances. The only source for additional vorticity needed to account for these large circulation fluctuations is the blade tip, and so we confirm the hypothesis of MD [16] that the inflow disturbances create unsteadiness in the leakage vortex by interfering with the shedding of vorticity from the blade tips.

At smaller tip gaps (1.65% and 0.83%c) the inflow unsteadiness produces a greater proportion of disturbances to the leakage vortex structure that are either directly associated with the inflow disturbances themselves, or directly produced by their impact on the leakage vortex. At the smallest tip gap (0.83%c) fluctuations in the vortex circulation are almost equal in amplitude to the strength of the inflow disturbances, implying that this direct interaction is the dominant mechanism.

Acknowledgements

The authors would like to thank the Office of Naval Research, in particular, Ki-Han Kim, for the support of this work through grant N00014-99-1-0294. The assistance of Nilanjan Saha, in setting up the wind tunnel and performing measurements, is gratefully acknowledged. Numerical results from the experiments described here are available from the authors' website.‡

References

[1] Poensgen, C., and Gallus, H. E., "Three-Dimensional Wake Decay Inside of a Compressor Cascade and Its Influence on the Downstream Unsteady Flow Field, Part 2 Unsteady Flow-Field Downstream of the Stator," *Journal of Turbomachinery*, Vol. 113, No. 2, 1991, pp. 190–197.

[2] Yamamoto, A., Mimura, F., Tominaga, J., Tomihisa, S., Outa, E., and Matsuki, M., "Unsteady Three-Dimensional Flow Behavior due to Rotor-Stator Interaction in an Axial Flow Turbine," ASME Paper 93-GT-404, 1993.

[3] Zeschky, J., and Gallus, H. E., "Effects of Stator Wakes and Spanwise Nonuniform Inlet Conditions on the Rotor-Flow," *Journal of Turbomachinery*, Vol. 115, No. 1, 1993, pp. 128–136.

[4] Gallus, H. E., Zeschky, J., and Hah, C., "Endwall and Unsteady Flow Phenomena in an Axial Turbine Stage," ASME Paper 94-GT-143, 1994; see also *Journal of Turbomachinery*, Vol. 117, No. 4, 1995, pp. 562–570.

[5] Wernet, M. P., John, W. T., Prahst, P. S., and Strazisar, A. J., "Characterization of the Tip Clearance Flow in an Axial Compressor Using Digital PIV," AIAA Paper 2001-00697, 2001.

[6] Wernet, M. P., Zante, D. V., Strazisar, T. J., John, W. T., and Prahst, P. S., "3-D Digital PIV Measurements of the Tip Clearance Flow in an Axial Compressor," ASME Paper GT-2002-30643, 2002.

[7] Zierke, W. C., Farrell, K. J., and Straka, W. A., "Measurements of the

‡Data available online at http://www.aoe.vt.edu/flowdata [retrieved 20 September 2004].

Tip Clearance Flow for a High-Reynolds-Number Axial-Flow Rotor," *Journal of Turbomachinery*, Vol. 117, No. 4, 1995, pp. 522–532.

[8] Zierke, W. C., Straka, W. A., and Taylor, P. D., "An Experimental Investigation of the Flow Through an Axial-Flow Pump," *Journal of Fluids Engineering*, Vol. 117, No. 3, 1995, pp. 485–490.

[9] Storer, J. A., and Cumpsty, N. A., "Tip Leakage Flow in Axial Compressors," *Journal of Turbomachinery*, Vol. 111, No. 2, 1991, pp. 252–259.

[10] Doukelis, A., Mathioudakis, K., and Papailiou, K., "The Effect of Tip Clearance Gap Size and Wall Rotation on the Performance of a High-Speed Annular Compressor Cascade," ASME Paper 98-GT-38, 1998.

[11] Muthanna, C., and Devenport, W. J., "The Wake of a Compressor Cascade with Tip Gap, Part 1. Mean Flow and Turbulence Structure," *AIAA Journal*, Vol. 42, No. 11, 2004, pp. 2320–2331.

[12] Wang, Y., and Devenport, W. J., "The Wake of a Compressor Cascade with Tip Gap, Part 2. Effects of Endwall Motion," *AIAA Journal*, Vol. 42, No. 11, 2004, pp. 2332–2340.

[13] Inoue, M., Kuroumaru, M., and Fukuhara, M., "Behavior of Tip Leakage Flow Behind an Axial Compressor Rotor," *Journal of Engineering for Gas Turbines and Power*, Vol. 108, No. 1, 1986, pp. 7–14.

[14] Inoue, M., and Kuroumaru, M., "Structure of Tip Clearance Flow in an Isolated Axial Compressor Rotor," *Journal of Turbomachinery*, Vol. 111, No. 3, 1989, pp. 250–256.

[15] Goto, A., "Three-Dimensional Flow and Mixing in an Axial Flow Compressor With Different Rotor Tip Clearance," *Journal of Turbomachinery*, Vol. 114, No. 3, 1992, pp. 675–685.

[16] Ma, R., and Devenport, W. J., "Unsteady Periodic Behavior of a Disturbed Tip Leakage Flow," *AIAA Journal*, Vol. 44, No. 5, 2006, pp. 1073–1086.

[17] Mish, P., Staubs, J., Intaratep, N., and Devenport, W. J., "Characterization of Unsteady Loading Occurring in a Linear Cascade Produced by Simulated Stator-Rotor Interaction," *16th International Symposium on Airbreathing Engines, Cleveland, OH*, 2003.

[18] Staubs, J., Mish, P., and Devenport, W. J., "Correlation Between Unsteady Loading and Tip Gap Flow Occurring in a Linear Cascade Produced by Simulated Stator-Rotor Interaction," *Proceedings of the ASME Heat Transfer/Fluids Engineering Summer Conference 2004*, HT/FED, ASME, New York, 2004, pp. 313–331.

[19] Ma, R., "Unsteady Turbulence Interaction in a Tip Leakage Flow Downstream of a Simulated Axial Compressor Rotor," Ph.D. Dissertation, Virginia Polytechnic Institute and State University, Blacksburg, VA, 2003.

[20] Wittmer, K. S., Devenport, W. J., and Zsoldos, J. S., "A Four-Sensor Hot-Wire Probe System for Three-Component Velocity Measurement," *Experiments in Fluids*, Vol. 24, Nos. 5–6, 1998, pp. 416–423.

[21] Kline, S. J., and McClintock, F. A., "Describing Uncertainties in Single Sample Experiments," *Mechanical Engineering*, Vol. 75, No. 1, 1953, pp. 3–8.

[22] Glegg, S. A. L., "The Response of a Swept Blade Row to a Three-Dimensional Gust," *Journal of Sound and Vibration*, Vol. 227, No. 1, 1999, pp. 29–64.

K. Ghia
Associate Editor